

New insights into ligand inductive effects on the stability of Mn₁₂ single-molecule magnets. Synthesis, magnetic and thermal characterization of complexes [Mn₁₂O₁₂(O₂CR)₁₆(H₂O)₄] \cdot xH₂O. (R = C₂H; x = 3 and R = C₂Ph; x = 4) and their thermolysis reaction products.

Jordi Gómez-Segura,^a Javier Campo,^b Inhar Imaz,^a Klaus Wurst,^c Jaume Veciana,^a Philippe Gerbier^{*c} and Daniel Ruiz-Molina^{*a}

^a Institut de Ciència de Materials de Barcelona (CSIC), Campus Universitari de la UAB, 08193 Bellaterra, Catalonia, Spain. Fax: +34 935805729; Tel: +34.935801853; E-mail: dani@icmab.es

^b Instituto de Ciencia de Materiales de Aragón (CSIC), Universidad de Zaragoza, 50009 Zaragoza, Spain. Fax: +34 976761229; Tel: +34 976762742; E-mail: jcampo@unizar.es

^c Allgemeine, Anorganische und Theoretische Chemie, Universität Innsbruck, Innrain 52a, A-6020, Innsbruck, Austria. Fax: +43(0)512/507-2934; Phone: +43(0)512/507-5145; E-mail: Klaus.Wurst@uibk.ac.at

^d Laboratoire de Chimie Moléculaire et Organisation du Solide, Université Montpellier II, C.C. 007, Place Eugène Bataillon, 34095 Montpellier, France. Fax: +33 467143852; Phone: +33.467143972; E-mail: gerbier@univ-montp2.fr

*This submission was created using the RSC Article Template (DO NOT DELETE THIS TEXT)
(LINE INCLUDED FOR SPACING ONLY - DO NOT DELETE THIS TEXT)*

Two novel Mn₁₂ derivatives [Mn₁₂O₁₂(O₂CC≡CH)₁₆(H₂O)₄] \cdot 3H₂O (**1**) and [Mn₁₂O₁₂(O₂CC≡CC₆H₅)₁₆(H₂O)₄] \cdot 3H₂O (**2**) have been prepared and characterized. Magnetic measurements confirm that both function as single-molecule magnets (SMM), showing frequency-dependent out-of-phase ac susceptibility signals and magnetization hysteresis curves. Thermal stability studies were first conducted in the solid state. While complex **1** undergoes a sudden exothermal decomposition ($T_{\text{onset}} = 118^\circ\text{C}$), complex **2** exhibits a stepwise degradation process leading to the production of manganese oxides at 500°C. Thermolysis reaction of **1** was hence assessed in solution to yield dark red crystals of a two-dimensional Mn^{II}-based co-ordination polymer [Mn₃(O₂CC≡CH)₆(H₂O)₄] \cdot 2H₂O (**3**), which corresponds to an extended sheet-like structure that crystallizes in the monoclinic space group P2₁/n; a = 9.2800(2) Å, b = 9.4132(2) Å, c = 14.9675(3) Å, $\beta = 99.630(1)^\circ$, and Z = 2. Finally, the magnetic properties of complex **3** have been studied on an oriented single crystal over two different orientations of the reciprocal vector versus the external field.

Introduction

The so-called single-molecule magnets (SMM) represent a new kind of nanoscopic molecular materials that offer potential access towards the ultimate high-density information storage devices and quantum computing applications.¹ Outstanding magnetic properties such as out-of-phase AC magnetic susceptibility signals and stepwise magnetization hysteresis loops are representative of an extensive number of large metal complexes that function as SMM. Different families of SMM have been so far reported based on manganese,² nickel,³ cobalt,⁴ iron⁵ and mixtures of metals.⁶ The well-known Mn₁₂ family possess one of the highest T_B so far reported (*ca.* 4K). Structurally, the metal core [Mn₁₂(μ_3 -O)₁₂] comprises a central [Mn^{IV}₄O₄]⁸⁺ cubane held within a non-planar ring of eight Mn^{III} ions by eight μ_3 -O₂⁻ ions. Peripheral ligation is provided by sixteen carboxylate groups that are amenable to variation and accomplished by three or four H₂O molecules.⁷ Small structural variations of the Mn₁₂ core induced by environmental and lattice network characteristics have been shown to significantly influence their magnetic properties and quantum tunnelling behaviour. For example, pure Jahn-Teller isomers of a given Mn₁₂ complex that crystallize in the same space group and differ only in the identity of one solvent molecule of crystallization at one position have been prepared and shown to exhibit different magnetization relaxation rates.⁸ Recent X-ray crystallographic studies have also shown that the presence of non-axial isomers in the crystal lattice of Mn₁₂ clusters may provide a possible

explanation for the intriguing tunnelling behaviour of single-molecule magnets.⁹

To gain more knowledge on how subtle structural modifications of the [Mn₁₂(μ_3 -O)₁₂] structure may influence the stability and magnetic properties of Mn₁₂ clusters, we have initiated a new synthetic strategy based on the systematic investigation of a number of Mn₁₂ complexes differing on the nature of peripheral carboxylic ligands. In previous works we have already presented a detailed study of the series CX₃CO₂H (X = F, Cl and Br), which exhibited a systematic variation of their volume and Lewis base character.^{10, 11} These studies showed that the relative thermal stability of Mn₁₂ complexes arises from an interplay between steric and ligand inductive effects.

In a further step, herein we present the synthesis, thermal study and magnetic characterization of two new Mn₁₂ clusters [Mn₁₂O₁₂(O₂CC≡CH)₁₆(H₂O)₄] \cdot 3H₂O (**1**) and [Mn₁₂O₁₂(O₂CC≡CC₆H₅)₁₆(H₂O)₄] \cdot 3H₂O (**2**). The propiolic acid of complex **2** was chosen on the basis of its remarkable acidity and small molecular volume.¹² Such a combination is expected to allow a specific study of the acidity effect on the thermal stability of the dodecamanganese core in the absence of remarkable steric congestions. Consequently, this is the ultimate step on the quest to elucidate the interplay between acidity and volume on the relative stability of Mn₁₂ clusters. Moreover, complex **3** bearing phenylpropionic carboxylate ligands, less acid but more bulky, has also been prepared for comparison purposes. Finally, the thermal stability of complexes **1** and **2** has been explored and the resulting information used to induce the thermal degradation of complex **1** into the new layered complex [Mn₃(O₂CC≡CH)₆(H₂O)₄] \cdot 2H₂O (**3**).

Experimental

All reagents and solvents were used as received and no further purification was carried out. Elemental analyses were performed by the Servei d'Anàlisi Química of the Universitat Autònoma de Barcelona. FT-IR spectra were collected on a Perkin Helmer spectrometer in the range of 400–4000 cm^{-1} as KBr discs. Complex **1** was synthesized as described in ref.¹³

Syntheses of complexes

[Mn₁₂O₁₂(O₂CC≡CH)₁₆(H₂O)₄]·3H₂O (1). To a solution of **4** (0.100g, 4·10⁻⁵ mol) in dichloromethane (5 ml) an excess (35 equiv.) of HC≡CCO₂H (0.100g, 1.4·10⁻³ mol) was added under stirring for few minutes. Isolation was achieved by slow diffusion of hexanes (5 mL) into this solution. Complex **1** was recovered as a brownish precipitate at the bottom of the diffusion tube. The solid was washed with dichloromethane and dried on a frit. Elemental analysis. Calc. for Mn₁₂C₄₈H₃₀O₅₁: C, 27.40; H, 1.43. Found: C, 27.02; H, 1.47. IR (KBr, cm^{-1}): 3439 (s), 3275 (s), 2109 (s), 1584 (s), 1400 (s), 1375 (s), 775 (m), 623 (m), 602 (m).

[Mn₁₂O₁₂(O₂CC≡CC₆H₅)₁₆(H₂O)₄]·4H₂O (2). Same procedure as described above, but replacing HC≡CCO₂H by C₆H₅C≡CCO₂H. Complex **2** was collected as small black needle-shaped crystals. The crystals were washed with pentane and dried in air. Elemental analysis. Calc. for Mn₁₂C₁₄₄H₉₆O₅₂: C, 52.11; H, 2.89. Found: C, 52.14; H, 2.88. IR (KBr, cm^{-1}): 3435 (s), 3056 (w), 2217 (s), 1569 (m), 1411 (s), 759 (m), 689 (m), 617 (m).

[Mn₃(O₂CC≡CH)₆(H₂O)₄]·2H₂O (3). Complex **1** (0.100g, 4.8·10⁻⁵ mol) were suspended in 5 ml of acetonitrile, heated to reflux for 5 min and left undisturbed at room temperature in an open Erlenmeyer flask. Complex **3** was collected as deep red rhombohedral crystals by slow evaporation of the solvent. The crystals were washed with a minimum amount of acetonitrile and dried on a frit. Elemental analysis. Calc. for Mn₃C₁₈H₁₈O₁₈: C, 31.44; H, 2.62. Found: C, 31.54; H, 2.66. IR (KBr, cm^{-1}): 3411 (m), 3270 (s), 2115 (s), 1714 (w), 1583 (s), 1540 (s), 1403 (s), 771 (m), 624 (m).

Crystallography

A rhombohedral X-ray quality crystal was selected and mounted on a Nonius Kappa CCD diffractometer equipped with monochromatic Mo K α ($\lambda = 0.71073\text{\AA}$) radiation. The structure of **3** was solved by direct methods, using SHELXTL¹⁴ software and refined by full-matrix least-squares method with SHELXTL software. The hydrogen atoms at carbon atoms were calculated, using a riding model, hydrogen atoms of water molecules were found and refined regular with isotropic temperature factors. All non-hydrogen. The details of the crystallographic data and refinement are summarized in Table 1.

Measurements

DC magnetic measurements were collected on a Quantum Design MPMS superconducting SQUID magnetometer equipped with a 5.5 T magnet and operational range of temperature 1.8–300 K. AC magnetic measurements were collected in a 1.0 Oe ac field at the frequencies 9–99 Hz with no applied dc field. TG/DTA measurements were simultaneously performed on a Setaram Labsys TG-TDA 12 thermogravimetric analyzer under an N₂ + O₂ flow (60 mL·min⁻¹) at a heating rate of 10 °C·min⁻¹

Results and Discussion

Synthesis and magnetic characterization of **1** and **2**

Complexes [Mn₁₂O₁₂(O₂CC≡CR)₁₆(H₂O)₄] \cdot xH₂O (**1**: R = H, x = 3; and **2**: R = C₆H₅, x = 4) were obtained following a synthetic methodology recently described by us.¹³ Such methodology is based on the use of complex [Mn₁₂O₁₂(O₂C^tBu)₁₆(H₂O)₄] (**4**) as the starting material for the ligand substitution reaction with the corresponding carboxylic acid (eq. 1). The presence of *tert*-butyl groups significantly increases its solubility in organic solvents and favours the displacement of the substitution equilibrium to completion due to the combined effects of the acidity and the steric demand.



Complex **1** was obtained as a brown microcrystalline powder at the bottom of the diffusion tube, being only moderately soluble in polar organic solvents such as acetonitrile. On the contrary, complex **2** was collected as small black crystals with a good solubility in a large variety of polar to weakly polar solvents. Unfortunately, these crystals gave too poorly resolved diffraction patterns to allow any further refinement, in spite of several recurrent crystallization experiments. Then, complexes **1** and **2** were characterized by elemental analysis, spectroscopic techniques and magnetic measurements.

AC magnetic susceptibility data were studied for polycrystalline samples of complexes **1** and **2** in the 1.8–10 K range with a 1 Oe ac field oscillating in the frequency range of 1–1150 Hz. The external dc magnetic field was held at zero. The resulting plot of the out-of-phase susceptibility χ'' signal versus temperature at three different frequencies is shown in Figure 1. As can be seen there, complex **2** exhibits frequency-dependent out-of-phase ac signals in the temperature range of 4–7 K whereas complex **1**

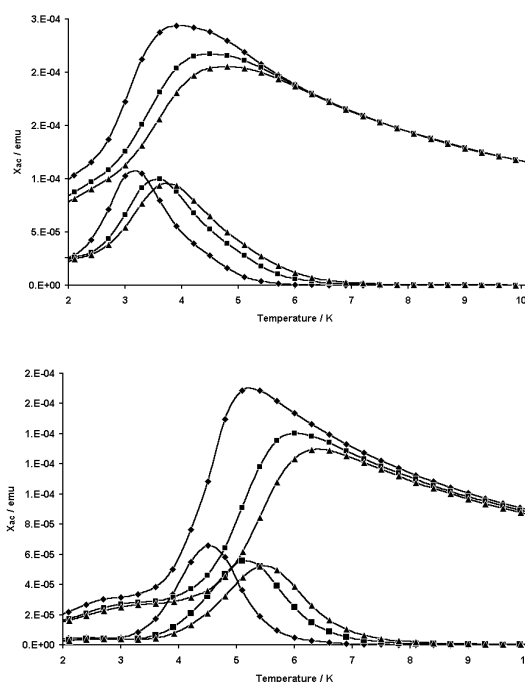


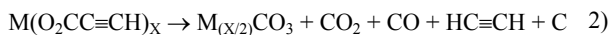
Fig.1 AC magnetic measurements for complex **2** (a) and **3** (b) in a 1 Oe ac field oscillating at the frequencies (♦) 2.11 (■) 5.7 and (▲) 11.1 Hz, with no applied dc field. The out of phase susceptibility (χ'') corresponds to the curves near the temperature axis in each plot. The in-phase curves (χ') have an higher response.

exhibits frequency-dependent out-of-phase ac signals in the temperature range of 2–4 K. The magnetization relaxation rate ($1/\tau$) determined from the position of the peak maximum follows the Arrhenius equation as expected for a thermally activated Orbach process with an energy barrier of 52.5 and 61.3 K for complexes **1** and **2**, respectively. Both, the observation of two different magnetization relaxation mechanisms (fast and slow relaxing species) and the respective effective energy barriers are characteristics of several other Mn_{12} complexes.^{Ref}

Magnetization hysteresis curves were also obtained for a polycrystalline sample of complexes **1** and **2** at three different temperatures (1.8, 2.0 and 2.5 K). The sample was oriented in eicosane such that the axial anisotropy axis of the molecule is parallel with the external field. The crystals were first added to eicosane and torqued in a 5 kOe field. The temperature was then raised above the melting point of eicosane (312–318 K), held there for 30 minutes and then reduced to room temperature. Because of the predisposition of the crystals to torque, the crystals were oriented such that the magnetoanisotropy axis (i.e., z-axis) of each molecule is parallel with respect to the external field. Then, samples are magnetically saturated in a +2.0 T field, and afterwards the field was swept down to -2.0 T, and cycled back +2.0 T. In the case of complex **1**, as the field is decreased from +2.0 T to zero, there is a considerable step at zero field that can be related with the predominance of the fast relaxing species rather than to the presence of thermally induced tunnelling. On the contrary, the magnetization hysteresis curves of complex **2** clearly exhibit steps on switching the external magnetic field. The presence of such steps has been already clearly attributed to resonance quantum mechanical tunnelling of the magnetization direction. If all the molecules changed their direction of magnetization by thermal activation over the barrier, then the hysteresis loop would be a smooth function with no steps.

Thermal studies

Thermogravimetric (TGA) and differential thermal analyses (DTA) experiments carried out on polycrystalline samples of complexes **1** and **2** are shown in Fig. 2. In the case of complex **2**, the DTA curve obtained by heating the sample at a constant rate of $10\text{ }^{\circ}\text{C}\cdot\text{min}^{-1}$ shows a single strong exothermic peak at $118\text{ }^{\circ}\text{C}$, accompanied by an abrupt weight loss in the corresponding thermogravimetric experiment. The resulting tiny brown material was associated with a decomposition product, as confirmed by IR spectroscopy. Indeed the IR spectrum of such brown material shows a pattern characteristic of $MnCO_3$, indicating that the exothermal process may be described by the following decarboxylation reaction (Eq. 2).¹²



The TGA and DTA curves of complex **2** are also shown in Fig. 2 (bottom). As can be seen there, the thermal response of complex **2** differs considerably from that observed for complex **1**. A first weight loss of 32 %, less abrupt than that of sample of **2** is characterized by two exotherms at $155\text{ }^{\circ}\text{C}$ and $192\text{ }^{\circ}\text{C}$, respectively. The second weight loss which begins at ca. $295\text{ }^{\circ}\text{C}$ corresponds to a weak exothermic process and leads at $500\text{ }^{\circ}\text{C}$ to a black residue, with an overall weight loss of 62.5 %. The first exothermic process may be attributed to a decarboxylation process, as previously described for complex **2**. However, in this case, the resulting phenylacetylenic radicals may react together on a polymerization process contributing in more or less degree to the thermal processes. The second weight loss, which begins at $295\text{ }^{\circ}\text{C}$, can be attributed to the decarboxylation reaction converting $MnCO_3$ into manganese oxides.

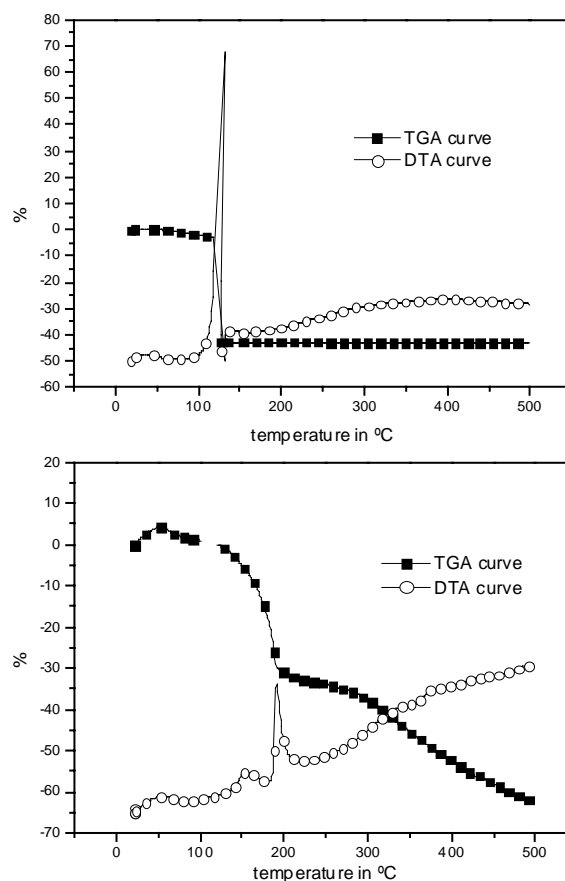


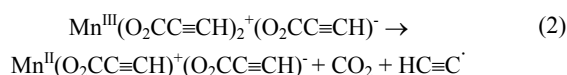
Fig. 2. TGA (plain symbols) and DTA (open symbols) curves of compounds **1** (top), **2** (bottom) in the temperature range 25–400 °C (heating rate: $10\text{ }^{\circ}\text{C}\cdot\text{min}^{-1}$) under an air flow.

Complexes **1** and **2** have pKa values of 1.84 and 2.25, respectively, and a comparable steric hindrance contribution (ca. $37\text{ }^{\circ}\text{Å}^3$).¹⁶ Therefore, the larger thermal stability of complex **2** may be well explained by the greater value of its pKa, i.e., its decreased inductive effect, confirming the importance of the pKa acidity on the thermal stability of the dodecamanganese core. In fact, the replacement of a hydrogen atom by a phenyl ring attached to a triple bond has already been shown to affect dramatically the reactivity of the latter, especially in the case of thermally-induced polymerizations.¹² Moreover, the temperature of decomposition of complexes **1** and **2** lies within the range of those described for other $[Mn_{12}O_{12}(O_2CR)_{16}(H_2O)_4]$ complexes, where R stands for $C(CH_3)_3$ ($T_d = 150\text{ }^{\circ}\text{C}$), CF_3 ($T_d = 130\text{ }^{\circ}\text{C}$) or $CHCl_2$ ($T_d = 110\text{ }^{\circ}\text{C}$).

Synthesis and structural characterization of complex 3

In a previous work we have already reported how the thermal treatment of some Mn_{12} clusters in solution leads to the obtaining of low nuclearity clusters by a decarboxylation process. For this reason, acetonitrile solutions of complexes **1** and **2** were also refluxed for 24 h under stirring and ambient conditions. As expected, the replacement of the acetylenic hydrogen atoms by a phenyl rings affects drastically the thermal stability of the Mn_{12} complexes not only in the solid state but also in solution. Indeed, whereas complex **2** remains unaltered during the thermal treatment, complex **1** experiences a thermally induced reaction, which on cooling, leads to the obtaining of a red-brown microcrystalline precipitate. Such precipitate was characterized as complex $[Mn_3(O_2CC\equiv CH)_6(H_2O)_4]$ (**3**) by elemental analysis and spectroscopic techniques. This implies a fragmentation of the metal core $[Mn_{12}(\mu_3-O)_{12}]$ with a reduction

of the mixed-valence Mn(III)Mn(IV) pattern into the Mn(II) oxidation state. This fact can be explained most likely via a catalytic decarboxylation mechanism in the presence of strong acids as described elsewhere.¹⁵ Co-ordinated carboxylates possessing a weak Lewis base character exhibit an appreciable lability that favours their release in solution. As a consequence, the metal core of the complex becomes co-ordinatively unsaturated—which, in turn, results in unstable cationic carboxylato-Mn^{III} species more sensitive to decarboxylation process via homolytic fragmentation (Eq. 2).¹⁵ Further aggregation of cationic carboxylato-Mn^{II} species yields the Mn^{II} trinuclear linear complex **4** (Eq. 3).



The recrystallization of **3** from boiling acetonitrile gave well-formed rhombohedral deep red crystals suitable for X-ray diffraction studies. The X-ray structural studies revealed that **3** crystallizes with two additional water molecules in an extended sheet-like structure with a monoclinic space group P2₁/n; *a* = 9.2800(2) Å, *b* = 9.4132(2) Å, *c* = 14.9675(3) Å, β = 99.630(1)°, and *Z* = 2 (Table 1) 2 and 203 parameters for 1889 reflections with *I* > 2σ(*I*). Crystallographic parameters are given on Table 1

Table 1: Crystallographic data for **3**

Formula	Mn ₃ C ₁₈ H ₁₈ O ₁₈
Formula weight	687.14
<i>T</i> /°C	223(2)
Crystal system	monoclinic
Space group	P2 ₁ /n
<i>a</i> /Å	9.2800(2)
<i>b</i> /Å	9.4132(2)
<i>c</i> /Å	14.9675(3)
β/°	99.630(1)
<i>V</i> /Å ³	1289.05(5)
<i>Z</i>	2
<i>D_c</i> /g cm ⁻³	1.77
μ(Mo-Kα)/mm ⁻¹	1.53
<i>R</i> 1	0.0193
<i>wR</i> 2	0.0486

As shown in Fig. 3a, complex **3** consists of a repetitive unit composed of three MnO₆ octahedra with a linear conformation. The central Mn(II) site of each trinuclear unit is connected to both lateral Mn(II) ions through six carboxylate ligands, whereas remaining coordinative positions of each external Mn ions are occupied by two water molecule ligands. Then, the basic trimeric units are connected to each other within the same plane to yield a 2-D structure (Fig 2b) consisting in a paving of hexamanganese pseudorectangular tiles, in which the organic groups are pointing toward the interior of the cavity.

A similar arrangement have been already found in two related extended complexes [Mn₃(O₂CCH₃)₄(H₂O)₄].8H₂O (**5**),¹⁷ and [Mn₃(O₂CCH₃)₆(H₂O)₄].2H₂O (**6**).¹⁸ In all the cases, the carboxylates link the central and the external ion of the trimeric unit via an μ-oxo bridge. Simultaneously, they are also bridging two Mn(II) ions of different trimeric units, through the O-C-O pathway with an *anti* configuration. As a result, the 2D organisation and the connection between the trimeric blocks are the same in all the cases.

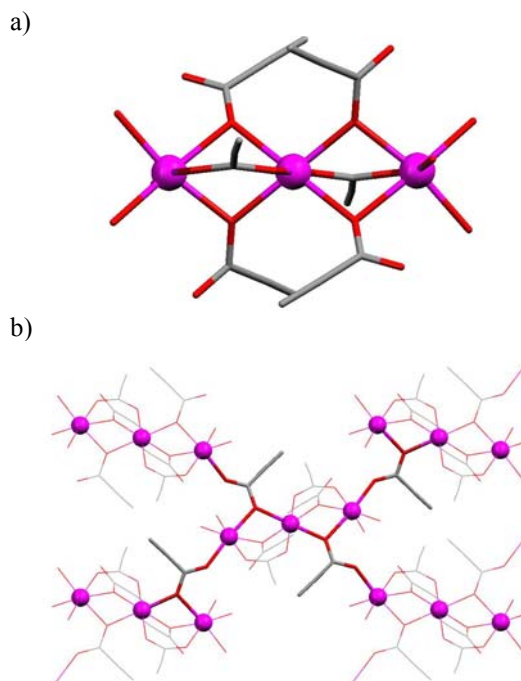


Fig. 3. a) View of the trimeric unit of compound **4**. b) View of the arrangement of the trimeric units in the bc-plane. Color keys, Pink: manganese atoms, red: oxygen atoms, gray: carbon atoms. Hydrogen atoms are not shown for sake of clarity.

However some differences can be highlighted, specially with the structure of complex **5**. In the Mn₃ core of **3** two of the six carboxylates exhibit a symmetrical syn-syn bridging mode, with bond distances of 2.129 and 2.193 Å that separates the Mn ions with a distance of 3.425 Å. The remaining four carboxylates exhibit a twofold coordination mode, within and between trimeric units. In the case of complex **5**, four of the six carboxylates are coordinated in the syn-syn mode to Mn ions. The remaining carboxylates are connected in a twofold coordination mode to the Mn ion located between them within the same trimeric unit and with Mn ions of neighbouring trimeric units.

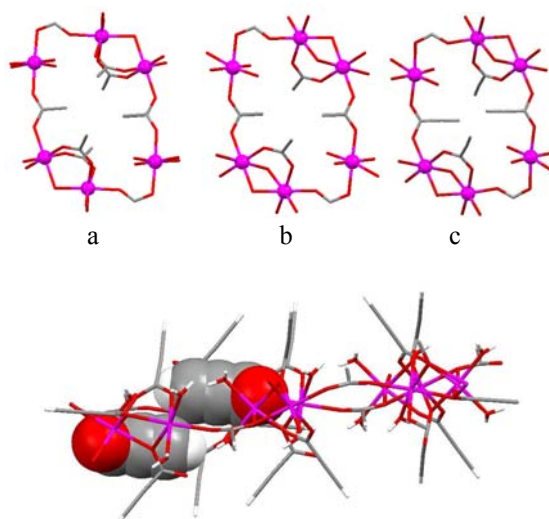


Fig. 4. (Top) View of the tiles in the plane showing the inner organic ligands: a) **5** b) **6**, and c) **3** structure. (Bottom) Side view of the tile for complex **3**, emphasizing the inner organic ligands by its representation with the space-filling model. Color keys, Pink: manganese atoms, red: oxygen atoms, gray: carbon atoms.

On the other side, the differences between complexes **3**, **5** and **6** come from the different steric constraints given by acetate and propionate groups. For comparison purposes, a top view of the tiles in the plane showing the inner organic ligands is shown in Fig. 4. Comparison of the transverse dimensions measured for the tiles of the structures shows that the tile size adapts to the steric hindrance generated by the inner organic groups directed to the centre of the tile. Interestingly, comparison of the constitutive tiles of **3** and **6** in the plane, shed some light on the reasons why such layered structures are obtained using propionic acid or acetic whereas linear polymeric¹⁹ or discrete molecular complexes (Mn₃, Mn₆) are characterized with other more bulky acids.^{10,11} From the examination of Fig. 4, it is clear that the cavity inside the tile can only accommodate ligands for which the van der Waals' volume does not exceed the value of *ca.* 37 Å³ (C₂H fragment).²⁰ With a volume slightly larger (43 Å³) the use of trifluoroacetate ligands leads to discrete complexes.²¹

Magnetic properties of complex **3**

Ac magnetic susceptibility data at different frequencies (0.1 < ν < 1k Hz range) and two orientations of the crystal with respect to the axis of the magnetometer, i.e. the applied magnetic field direction, were obtained for a single crystal of **3**. In one of the orientations, the reciprocal vector [10-1]*, which is perpendicular to the layers of polymeric Mn trimers, lies perpendicular whereas in the other one lies parallel to the axis of the magnetometer. The ac susceptibility curves for both orientations are shown in Fig. 5.

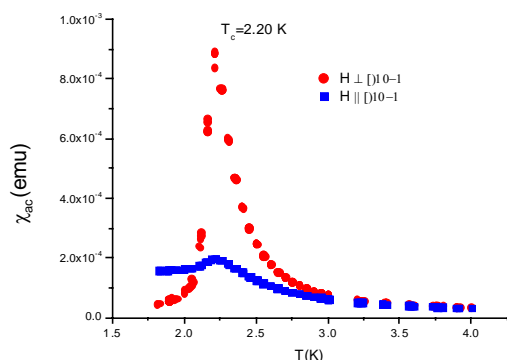


Fig. 5. In-phase ac susceptibility curves vs. temperature at different frequencies (*que frecuencias?*) measured for two orientations of a single crystal of **3**.

As can be seen in Fig. 5, the in-phase signal exhibits a peak at 2.2 K associated to the presence of long range magnetic order. The stronger signal of the peak, which does not exhibit any frequency dependence, was obtained when the reciprocal vector [10-1]* lies perpendicular to the axis of the magnetometer. This fact can be explained by the presence of stronger fluctuations or predominant ferromagnetic interactions within the polymeric layers, whereas antiferromagnetic interactions take place between different layers, i.e., when the reciprocal vector [10-1]* lies parallel to the axis of the magnetometer. Such assignation can be justified by considering the structural arrangement of complex **3**. Indeed, according with the linear disposition of the Mn²⁺ cations within the repetitive trimeric unit, it is expected that the Mn ion with double multiplicity couples antiferromagnetically with each Mn ion located on a fourfold multiplicity site, leading to a ferrimagnetic entity with a spin $S=5/3 \mu_B$, as described by the Hamiltonian,

$$H = -2(J_{1,2}\mathbf{S}_1 \cdot \mathbf{S}_2 + J_{2,3}\mathbf{S}_2 \cdot \mathbf{S}_3 + J_{3,1}\mathbf{S}_3 \cdot \mathbf{S}_1)$$

where $S_i = 5/2$ and $J_{1,2}$ is negative and $J_{3,1}$ is equal to zero.

Then, the resulting net magnetic moment $S=5/3$ of each trimeric unit couple ferromagnetically between them along the 2-D layers, which in turn couple antiferromagnetically to each other leading to a 3-D long range magnetic order below 2.2 K.

Variable-temperature dc magnetization measurements of a single crystal oriented with the reciprocal vector [1 0 -1]* perpendicular to the external magnetic field, have also been measured as function of temperature at several different magnetic fields ranging from 20 Oe to 10 kOe. The resulting magnetization curves, normalized by the applied external field, are shown in Fig. 6. At low fields ($H < 150$), the sample experiences a transition from a paramagnetic to an antiferromagnetic phase (antiferromagnetically coupled planes). However, an increase of the magnetic field over 0.1 kOe induces variations on the magnetization curves. In this case, the magnetic phase transition is associated with a transition from a paramagnetic to a ferrimagnetic phase (ferromagnetic interactions within the layer). Finally, an increase of the external magnetic field over 10 kOe induces a systematic decrease of the susceptibility moment (M/H) most likely due to saturation effects.

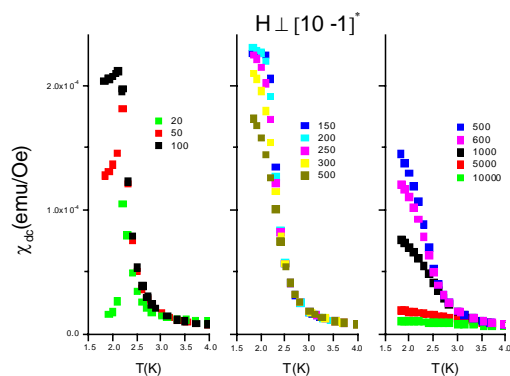


Fig. 6. Dc susceptibility curves vs. Temperature at different constant magnetic fields measured for two orientations of a single crystal of **4**

Finally, magnetization versus magnetic field measurements was carried out at 1.8 K for two different orientations of the crystal (see Fig. 7). From there, two main conclusions can be extracted. First, at magnetic fields higher than 3 kOe ($H > 3\text{kOe}$) the magnetization curves for both orientations are similar, as can be observed in the upper insert of the Fig. 7. From the same figure, we may also extract the second important detail about the easy axis of magnetization, which must be contained within the polymeric layers. Another remarkable fact is that at fields $H > 30$ kOe the crystal increases its magnetization showing that the ferrimagnetic triplets are passing from the fundamental state to an energy level with higher magnetic moment before reaching complete saturation, apparently for fields $H > 55$ kOe (not measurable in our experimental set-up). Finally, in the low field region ($H < 50$ Oe) we can notice that both curves are similar whereas for $50 \text{ Oe} < H < 3 \text{ kOe}$ the curves split. The magnetic structure in the ordered state cannot be determined from this limited experimental set of macroscopic measurements. As previously mentioned, a simple model that justifies such results is that the Mn₃ trimers couple antiferromagnetically to give a net ferrimagnetic moment, which in turn interacts ferromagnetically with other trimers of the same layer. Finally the layers interact antiferromagnetically with other layers giving an antiferromagnetic structure at zero field. The direction of the magnetic moment lies inside the layer although a weak canting (one layer with its neighbours) cannot be excluded. Then, when a magnetic field is applied perpendicular to the [1 0 -1]* direction a metamagnetic phase transition occurs for fields

higher than 50 Oe due to the very low anisotropy of the Mn trimers. If the magnetic field is applied along to the $[1\ 0\ -1]^*$ vector then the system reaches gradually the saturated state. However, to fully verify this hypothesis, further neutron diffraction experiments to resolve the magnetic structure are currently underway.

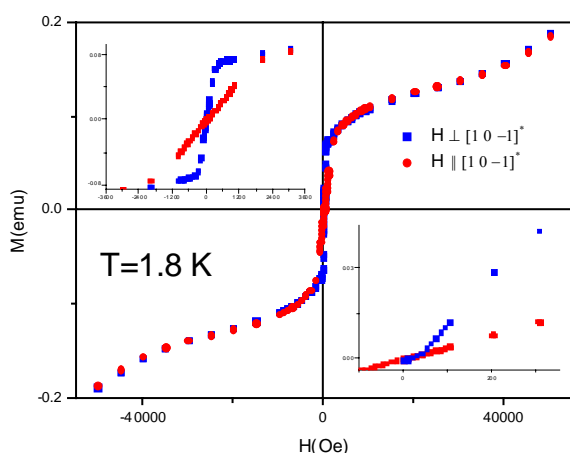


Fig. 7. Magnetization versus magnetic field isotherms at 1.8 K measured for two orientations of a single crystal of **4**

Conclusions

Propiolic acid comprises an unsaturated organic chain attached to the carboxylate group CO_2^- . On the basis of the linear structure, steric hindrance between adjacent carboxylates in the coordination sphere is highly minimized. As a consequence, any disruption of the $[\text{Mn}_{12}(\mu_3\text{-O})_{12}]$ core is prone to be originated mostly by marked inductive effects due to its dissociation constant ($\text{pK}_a=1.84$), i.e. weak Lewis base character. As a consequence, complex **2** results in a lower thermal stability than that of the phenyl derived carboxylate ($\text{pK}_a=2.25$), favouring oxidative decarboxylation process. In contrast to complex **2**, the corresponding phenylpropionate Mn_{12} complex shows a wider thermal stability domain and side reactions involving phenyl radicals are unlikely to undergo explosive degradation.

The magnetic measurements performed on the new complexes **2**, **3**, show a characteristic behaviour of Mn_{12} Single Molecule Magnet. On the other hand, the model deduced from our magnetic results measurements obtained with the two-dimensional **4** complex shows an interesting intralayer ferrimagnetic behaviour resulting from the antiferromagnetic coupling inside Mn_3 cores and ferromagnetic interactions between the trimeric units. The layers interact antiferromagnetically between them.

Acknowledgements

This work was supported by the Spanish government under MAT 2002-0043, the Generalitat de Catalunya under XI2002-9 and the EU under the project Nanomagiqc. P. G. is grateful to the Région Languedoc-Roussillon for its financial support through the Communauté de Travail des Pyrénées network DeNaMol. D. R.-M. also wants to thank Prof. David Hendrickson for fruitful discussions on the chemistry of Mn_{12} clusters.

References

- G. Christou, D. Gatteschi, D.N. Hendrickson and R. Sessoli, *MRS Bull.* 2000, **25**, 56; D. Gatteschi and R. Sessoli, *Angew. Chem. Int. Ed.* 2003, **42**, 268.
- C. Boskovic, W. Wernsdorfer, K. Folting, J.C. Huffman, D.N. Hendrickson and G. Christou *Inorg. Chem.* 2002, **41**, 5107 (and referenced cited therein).
- C. Cadiou, M. Murrie, C. Paulsen, V. Villar, W. Wernsdorfer and R.E.P. Winpenny, *Chem. Commun.* 2001, **24**, 2666.
- E.C. Yang, D.N. Hendrickson, W. Wernsdorfer, M. Nakano and G. Christou, *J. Appl. Phys.* 2002, **91**, 7382.
- C. Sangregorio, T. Ohm, C. Paulsen, R. Sessoli and D. Gatteschi, *Phys. Rev. Lett.* 1997, **78**, 4645; A.L. Barra, A. Caneschi, A. Cornia, F.F. De Biani, D. Gatteschi, C. Sangregorio, R. Sessoli and L. Sorace, *J. Am. Chem. Soc.* 1999, **121**, 5302.
- J.J. Sokol, A.G. Hee and J.R. Long, *J. Am. Chem. Soc.* 2002, **124**, 7656.
- D. Ruiz-Molina, G. Christou and D.N. Hendrickson, *Mol. Cryst. Liq. Cryst.* 2000, **343**, 17.
- M. Soler, W. Wernsdorfer, Z. Sun, J. C. Huffman, D. N. Hendrickson and G. Christou, *Chem. Comm.* 2003, 2672.
- A. Cornia, A. C. Fabretti, R. Sessoli, L. Sorace, D. Gatteschi, A. L. Barra, C. Daiguebonne and T. Roisnel, *Acta Cryst.* 2002, **C58**, 371.
- Ph. Gerbier, D. Ruiz-Molina, J. Gómez, K. Wurst, J. Veciana, *Polyhedron*, 2003, **22**, 1951.
- J. Gómez-Segura, E. Lhotel, C. Paulsen, D. Luneau, K. Wurst, J. Veciana, D. Ruiz-Molina, Ph. Gerbier, *New. J. Chem.* 2005, **3**, 499.
- C. E. Stoner, Jr, T. B. Brill, *Inorg. Chem.* 1989, **28**, 4500.
- P. Gerbier, D. Ruiz-Molina, N. Doming, D. B. Amabilino, J. Vidal-Gancedo, J. Tejada and J. Veciana, *Monatsh. Chem.* 2003, **134**, 265.
- G. M. Sheldrick, University of Goettingen: Goettingen, **1997**
- J.M. Anderson, J. K. Kochi, *J. Am. Chem. Soc.* 1970, **92**, 2450.
- Y. H. Zhao, M. H. Abraham, A. M. Zissimos, *J. Org. Chem.* 2003, **68**, 7368.
- E. F. Bertaut, T. Q. Duc, P. Burlet, P. Burlet, M. Thomas, J.-M. Moreau, *Acta Cryst.* 1974, **B30**, 2234.
- C. -Y. Cheng and S. -L. Wang, *Acta Cryst.* 1991, **C47**, 1734.
- T. Lis, *Acta Cryst.* 1977, **B33**, 2964.
- Except for the formate ligands which lead to 3-D networks: M. Viertelhaus, H. Henke, C. E. Anson, A. K. Powell, *Eur. J. Inorg. Chem.* 2003, 2283.
- H. Zhao, C. P. Berlinguette, J. Bacsá, S. E. Tichy, K. R. Dunbar, *J.Cluster Sci.* 2003, **14**, 235.

